Quantitative analyses of regional [^{11}C]PE2I binding to the dopamine transporter in the human brain: a PET study

Aurelija Jucaite[2], Ikuo Odano[3], Hans Olsson[1], Stefan Pauli[1], Christer Halldin[1], Lars Farde[1]

[1] Psychiatry Section, Department of Clinical Neuroscience, Karolinska Institutet, Stockholm, Sweden
[2] Department of Woman and Child Health, Karolinska Institutet, Stockholm, Sweden
[3] Division of Functional Imaging, Department of Sensory and Integrative Medicine, Niigata University Graduate School of Medicine and Dental Sciences, Asahimachi-dori Niigata, Japan

Received: 20 November 2005 / Accepted: 20 November 2005 / Published online: 3 March 2006

Abstract. *Purpose:* The dopamine transporter (DAT) is a plasma membrane protein of central interest in the pathophysiology of neuropsychiatric disorders and is known to be a target for psychostimulant drugs. [^{11}C]PE2I is a new radioligand which binds selectively and with moderate affinity to central DAT, as has been demonstrated in vitro by autoradiography and in vivo by positron emission tomography (PET). The aims of the present PET study were to quantify regional [^{11}C]PE2I binding to DAT in the human brain and to compare quantitative methods with regard to suitability for applied clinical studies.
Methods: One PET measurement was performed in each of eight healthy male subjects. The binding potential (BP) values were obtained by applying kinetic compartment analysis, which uses the metabolite-corrected arterial plasma curve as an input function. They were compared with the BP values quantified by two reference tissue approaches, using cerebellum as a reference region representing free and non-specific radioligand binding.
Results: The radioactivity concentration was highest in the striatum, lower in the midbrain and very low in the cerebellum. The regional [^{11}C]PE2I binding could be interpreted by kinetic compartment models. However, the BP values in the striatum obtained by the compartment analyses were about 30% higher than the BP values obtained using reference tissue methods. We suggest that the difference may be explained by the inaccurate metabolite correction, small amounts of radioactive metabolites that could account for the presence of non-specific binding in the cerebellum and insufficient data acquisition time.
Conclusion: The reference methods may be used to quantify [^{11}C]PE2I binding in clinical studies, assuming that non-specific binding in the cerebellum does not vary between subjects and that an extended data acquisition time is employed. Moreover, the study corroborates the previous observation that [^{11}C]PE2I is advantageous for PET examination of DAT binding in the midbrain, a region from which dopaminergic innervation originates and which is of central interest for the pathophysiology of several neuropsychiatric disorders.

Keywords: Dopamine transporter – Substantia nigra – Human – PET – Kinetic modelling

Eur J Nucl Med Mol Imaging (2006) 33:657–668
DOI 10.1007/s00259-005-0027-9

Aurelija Jucaite (✉)
Department of Woman and Child Health,
Karolinska Institutet,
Stockholm, Sweden
e-mail: aurelija.jucaite@kbh.ki.se
Tel.: +46-8-51777503, Fax: +46-8-51777349

Introduction

The dopamine transporter (DAT) protein is localised on cell membranes of dopaminergic neurons and highly expressed in the striatum. The main physiological function of the DAT is to regulate the dopamine concentration in the synapse by high-affinity presynaptic reuptake [1].

Molecular imaging studies have reported changes in the density and function of DAT in vivo in a number of neuropsychiatric disorders, such as Parkinson's disease [2], Huntington's disease [3], schizophrenia [4] and attention deficit/hyperactivity disorder [5, 6]. In addition, DAT has served as a marker of dopaminergic terminals in research on the pathophysiology of drug abuse and modes of psychostimulant action [7].

The recognition of a role of the DAT in physiological as well as pathophysiological conditions has stimulated development of suitable radioligands for imaging by positron

emission tomography and single-photon emission computed tomography (PET and SPECT). However, most hitherto developed radioligands have been non-selective, i.e. they also have affinity for the serotonin and noradrenaline transporters. In the search for improved ligands, PE2I [*N*-(3-iodoprop-2*E*-enyl)-2β-carbomethoxy-3β-(4-methylphenyl) nortropane] has been synthesised, and has been shown to have nanomolar affinity to the DAT and approximately 10 and 30 times lower binding affinity to the noradrenaline and the serotonin transporter, respectively [8]. Autoradiographic studies on large-scale cryosections from the human brain have confirmed the selectivity of [^{125}I]PE2I binding to DAT and demonstrated high [^{125}I]PE2I binding in the striatum, intermediate binding in the midbrain and no binding in the cerebellum or neocortex [9].

We have recently reported on the radiolabelling of PE2I with carbon-11 and preliminary PET measurements in a monkey and a man [10]. Displacement and pre-treatment measurements in the monkey brain confirmed that [^{11}C]PE2I binds selectively and reversibly to the DAT in vivo. Interestingly, in this preliminary study there was conspicuous accumulation of [^{11}C]PE2I in the midbrain region—the substantia nigra and ventral tegmental area. This region contains dopaminergic cell bodies and is implicated in degenerative brain disorders, such as Parkinson's disease.

The aims of the present study were to quantify the regional binding of [^{11}C]PE2I and to evaluate its suitability as a PET radioligand for applied studies in human subjects. Initially, a metabolite-corrected arterial plasma input function was used in kinetic compartment analyses. The binding potential (BP) values were compared with those obtained by kinetic and reference tissue approaches in order to select the most appropriate method for further clinical studies.

Materials and methods

Theory of quantitative approaches for binding parameters

For cross-validation purposes, the time-activity curves (TACs) for [^{11}C]PE2I binding were interpreted using several established quantitative approaches. Kinetic compartment analyses and linear graphical analysis are two approaches dependent on a metabolite-corrected arterial plasma curve as input function. The simplified reference tissue model and linear graphical analysis using cerebellum as an input function are referred to as reference tissue approaches.

Kinetic compartment analyses

The three-compartment model (3-CM)

[^{11}C]PE2I was assumed to be freely diffusible from the blood pool to brain tissue. A conventional way to evaluate radioligand binding to receptors in brain is to use the four-compartment model shown in Fig. 1 [11].

The four compartments correspond to the radioactivity concentrations of unchanged radioligand in plasma (C_p), free (unbound) radioligand in brain (C_f), non-specifically bound radioligand in brain (C_{ns}) and radioligand specifically bound to transporter protein (C_b).

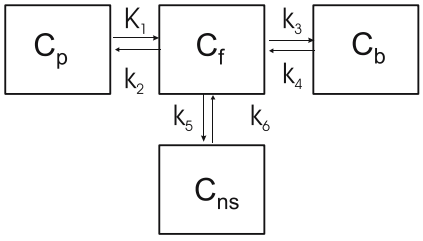

Fig. 1. Four-compartment model

Six rate constants are used to model tracer uptake. The rate constants K_1 and k_2 correspond to the influx and outflux rates for radioligand diffusion through the blood-brain barrier, respectively. The rate constants k_3 and k_4 correspond to the rates for radioligand transfer between the compartments for free (C_f) and specifically bound (C_b) radioligand, respectively. The rate constants k_5 and k_6 correspond to the rates for radioligand transfer between the compartments for free and non-specifically bound radioligand, respectively. It was assumed that all compartments are homogeneous in concentration. All concentrations are expressed in units of nCi/ml; K_1 has units of ml/ml/min of brain tissue, and k_2 through k_4 have units of min^{-1}. All values of kinetic constants were expressed as mean±SD.

A common assumption is that the rate constants k_5 and k_6, describing exchange between C_f and C_{ns}compartments, are very fast. These two compartments can thus be treated as one compartment representing non-displaceable radioligand in brain, C_n [12]. Thereby the simplified model has three compartments (3-CM) and the four rate constants, K_1, k_2, k_3 and k_4 [12–14], and has been used to describe the time course of regional [^{11}C]PE2I binding in the striatum and midbrain.

On the basis of this model, the following first-order differential equations can be expressed:

$$\frac{dC_n(t)}{dt} = K_1 \cdot C_p(t) - (k_2 + k_3) \cdot C_n(t) + k_4 \cdot C_b(t), \quad (1)$$

$$\frac{dC_b(t)}{dt} = k_3 \cdot C_n(t) - k_4 \cdot C_b(t), \quad (2)$$

and

$$C^{PET}_{tissue}(t) = C_n(t) + C_b(t), \quad (3)$$

where $C^{PET}_{tissue}(t)$ is the net radioactivity concentration in brain obtained by the PET system.

The four rate constants were determined by curve fitting with a non-linear least squares fitting technique using the Simplex algorithm [15] with constraints restricting parameters between 0 and 0.9. Each initial value for K_1, k_2, k_3 and k_4 was 0.5, 0.1, 0.5 and 0.5, respectively. The local minimum of the sum of the squared residuals was determined by iteration. The time course for radioactivity of unchanged [^{11}C]PE2I in arterial plasma, i.e. the metabolite-corrected arterial plasma curve [$C_p(t)$] was used as the input function and the uncorrected arterial whole blood curve [$C_a(t)$] was employed to estimate the radioactivity contribution from the cerebral blood volume (CBV). The CBV was corrected for using the following equation:

$$C_{pet}(t) = C^{PET}_{tissue}(t) + \alpha \cdot CBV(t), \quad (4)$$

where $C_{pet}(t)$ represents the radioactivity measured by the PET system and α represents the fractional volume of blood present in the tissue volume, which was assumed to be 0.04 [16–19].

Derived parameters

Distribution volume Regional [^{11}C]PE2I binding was also expressed using the concept of the total distribution volume (DV_{total}), which is defined by the following equation, using kinetic constants obtained from the 3-CM [18, 20, 21]:

$$DV_{total} = \frac{K_1}{k_2} \cdot \left(1 + \frac{k_3}{k_4}\right). \quad (5)$$

Binding potential Since we use a radioligand with high specific radioactivity, the receptor density (B_{max}) and affinity (K_d) cannot be differentiated [13]. The B_{max} to K_d ratio corresponds to the k_3 to k_4 ratio in the 3-CM, which is referred to as binding potential [13]. The binding potential (BP) is defined as follows:

$$BP = \frac{k_3}{k_4} \quad (6)$$

Only a small fraction of the radioligand is truly free in plasma (f_1) and tissue (f_2). Eq. 6) is thus a simplification of the more elaborate expression:

$$BP = f_2 \cdot k_3/k_4 = f_2 \cdot B_{max}/K_d \quad (7)$$

In the present study the free fractions were not measured; we assumed that f_1 and f_2 are not time dependent.

The two-compartment model (2-CM)

If the binding and release of [^{11}C]PE2I from the specific binding compartment (C_b) are rapid compared with the transport parameters K_1 and k_2, the model can be further reduced to two compartments (2-CM). Here a single tissue compartment contains free, non-specifically bound and specifically bound ligand [18]. In this manner, the kinetic parameters are reduced to only two, $K_1$and k_2'.

To determine which compartment model better describes the [^{11}C]PE2I binding in the brain, we compared the models using three statistical methods: the Akaike information criterion [22], the Schwarz criterion [23] and *F* statistics [24].

Linear graphical analyses

Linear graphical analysis (arterial input)

[^{11}C]PE2I binding was analysed using a linear graphical analysis for reversible ligand binding [25]. The regional distribution volumes (DV_{Logan}) were determined from the slope of the linear plots obtained from 24 to 60 min after i.v. injection (time of the mid-frame) using the radioactivity of unchanged [^{11}C]PE2I in arterial plasma as an input function. This starting time point was chosen as there was no significant difference in the slope of the line when comparing the interval starting from 24 min with the intervals starting at later times (data not shown). The CBV correction was performed using Eq. 4. The binding potential $BP_{Logan(kinetic)}$ was calculated using the following equation:

$$BP_{Logan(kinetic)} = \frac{DV_{ROI}}{DV_{crb}} - 1 \quad (8)$$

Linear graphical analysis (reference tissue approach)

If C_n in the target tissue can be estimated from a reference region and if C_b in the reference region is negligible, the distribution volume ratio (DVR) can be obtained independently of blood data [25]. In the present study, cerebellum was chosen as the reference region since it has been shown that there is a negligible dopamine transporter density in this region [9, 10]. Under these conditions, the binding potential ($BP_{Logan(reference)}$) can be calculated as follows:

$$BP_{Logan(reference)} = DVR - 1$$

The time period used for the linear fit was from 42 to 60 min (time of the mid-frame).

The simplified reference tissue model (SRTM)

If the rate constant ratio is the same in the target tissue as obtained by the 3-CM (K_1/k_2) and in the reference tissue as obtained by the 2-CM (K_1/k_2'), and the tracer kinetics in the cerebellum may be described by the 2-CM, BP is obtained by solving the convolution equation using a non-linear least squares fitting technique [21]. This model requires no arterial blood sampling. We used the simplified version of this model [26] in which the tissue region of interest is approximated to a single compartment and the parameters required for a model fit are thereby reduced to three: R_1 (delivery relative to the reference tissue), k_2 (the rate constant from tissue to plasma) and BP.

Subjects

Eight male subjects, aged 19–38 years, participated in the study after signing written informed consent in accordance with the Helsinki Declaration. They were healthy according to medical history, physical examination, blood screening analysis and magnetic resonance imaging (MRI) of the brain and did not use any medication. There was no history of psychiatric disorder or drug abuse. The study was approved by the Research Ethics and Radiation Safety Committees of the Karolinska Hospital.

MRI and head fixation system

The anatomical MR images were acquired using the MRI system GE Signa unit (Milwaukee, WI), 1.5 Tesla. A standard spin-echo sequence with a 512×256 matrix was used with a repetition time of 400 ms. Echo times were 9 ms for T1-weighted images. A head fixation system with an individual plaster helmet was used for both MRI and PET measurements to optimise and standardise head position in the two imaging modalities. This experimental procedure may be viewed as a "co-registration procedure" before data processing and has an estimated precision of ≤2 mm [27].

Radiochemistry

The acid precursor of PE2I was prepared and radiolabelled by O-methylation using [^{11}C]methyl triflate as described in detail elsewhere [10]. The decay-corrected radiochemical yield of [^{11}C]PE2I was 50%. The radiochemical purity of the final product was >99%. The specific radioactivity of [^{11}C]PE2I at the time of injection was between 521 and 2,119 Ci/mmol (mean 1,094 Ci/mmol, *n*=8). The radioactivity injected ranged from 4.9 to 7.6 mCi (mean 5.9 mCi) and the injected mass was between 1.42 μg and 5.89 μg (mean 3.71 μg).

PET experimental procedure

In each PET measurement the subject was placed recumbent on a bed with his head in the PET system. A cannula was inserted into the right cubital vein and another cannula into the left brachial artery. A sterile physiological phosphate buffer (pH 7.4) solution containing [^{11}C]PE2I was injected as a bolus during 2 s into the cubital vein. The cannula was then immediately flushed with 10 ml saline.

Radioactivity in brain was measured for 63 min. Acquisition started immediately after intravenous injection according to a pre-programmed sequence of 15 frames. The frame sequence consisted of three 1-min frames followed by four 3-min frames and eight 6-min frames.

The PET system used was Siemens ECAT Exact HR, which provides 47 sections with a centre to centre distance of 3.125 mm. The intrinsic spatial resolution was 3.8 mm in plane and 4.0 mm full-width at half-maximum (FWHM) axially [28]. The images were reconstructed with a Hanning filter, 2.0 mm FWHM. The image matrix size was 128×128×47, and the voxel size was 2.02×2.02× 3.125 mm. The image resolution was 5 mm in plane and 6 mm axially. Attenuation correction was done using the transmission scan data obtained for each subject before PET measurements. Scatter correction and corrections for random counts and deadtime were applied.

Arterial blood sampling

To obtain the arterial input function, an automated blood sampling system was used for continuous (counts/second) plasma radioactivity measurements during the first 5 min of the PET measurement [29]. Subsequent arterial blood samples were taken manually at the midpoint of each frame until the end of PET data acquisition. The difference between appearance of radioactivity in the automated blood sampling system and brain was approximately 10 s.

Determination of radioactive metabolites in plasma

Arterial blood samples (2 ml) were drawn at set times: 4, 10, 20, 30, 40 and 50 min after i.v. injection of [^{11}C]PE2I. The supernatant liquid obtained after centrifugation for 2 min was deproteinised with acetonitrile. It was then analysed by gradient high-performance liquid chromatography (HPLC) on a reverse-phase column (Waters μ-Bondapak C18, 7.8×300 mm, 10 μm) and eluted at 6 ml/min over 9 min with acetonitrile/0.01 mol/l phosphoric acid, using gradient of 10/90 to 70/30 acetonitrile from 0 to 6.5 min and back to 10/90 at 7.5 min. The fractions of plasma radioactivity corresponding to unchanged [^{11}C]PE2I were determined as has been described previously [10], identifying similar, more polar metabolites of [^{11}C]PE2I .

Regions of interest

Regions of interest (ROIs) for the caudate nucleus, putamen, thalamus, midbrain, frontal and temporal cortices, cerebellar cortex and the whole brain contour were drawn on MR images in three adjacent axial sections. The choice of ROIs was guided by the known regional DAT expression in vitro [9] and visualisation using volume-rendered images (Fig. 2). The sets of ROIs were manually transferred to the reconstructed PET summation images using anatomical landmarks as a guide. The data were pooled to obtain the average radioactivity concentration for the whole volume of interest. To obtain regional time-activity curves (TACs), regional radioactivity was calculated for each frame, corrected for decay and plotted over time.

To calculate the percentage of [^{11}C]PE2I injected that was present in brain at the time of maximal radioactivity, the radioactivity concentration in the ROI of whole brain was multiplied by the estimated average brain volume (1,250 ml) and divided by the radioactivity injected and multiplied by 100 to obtain the percentage.

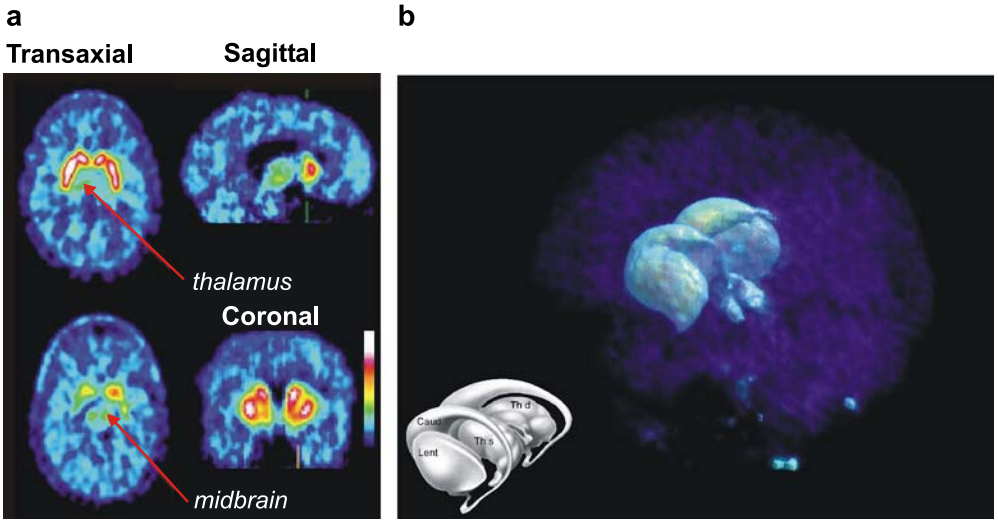

Fig. 2. a Summated PET images (9–63 min) showing the brain distribution of radioactivity in three projections after intravenous injection of [^{11}C]PE2I in an adult subject. Transaxial projections are presented at the level of the basal ganglia and at the upper midbrain. *Arrows* indicate [^{11}C]PE2I binding in the thalamus and midbrain. **b** Volume-rendered PET image showing the human brain distribution of radioactivity of [^{11}C]PE2I in an adult subject. Clearly visible is the binding to the caudate (*Caud*) and putamen (*Put*) structures. The midbrain structure (substantia nigra/ventral tegmentum, *SN/VTA*) is easily identified as the structure behind and below the caudate-putamen. In addition, some binding is seen in the hypothalamus and thalamus, but there is no binding in the neocortex. Inserted is the schematic drawing of the striatum and thalamus, indicating analogous brain structures and the thalamus (*Th s* and *Th d*, left and right side, respectively). It is adapted from: Nieuwenhuys R, Voogd J, van Huijzen C. The human central nervous system. A synopsis and atlas 3rd ed. Springer-Verlag: 1988; p. 30, Fig. 26 (Copyright permission granted)

Volume rendering

The distribution of the dopamine transporter in the human brain was visualised using a volume-rendering technique [30, 31]. It aimed to inspect the different areas of the brain and to choose ROIs for further quantitative analysis. This technique has previously been described in detail in a PET study on benzodiazepine receptor binding in the human brain [32].

In short, the basic concept in volume rendering is that each volume element, voxel, is projected onto an image screen. Each voxel is assigned a colour and opa, both of which are related to the radioactivity in the corresponding data point. The PET data frames corresponding to the time interval from 9 to 63 min were summed into one 3D voxel matrix and used for volume rendering.

Results

After intravenous injection of [^{11}C]PE2I, the TACs for total brain radioactivity rapidly reached a peak, which appeared during the frame from 3 to 6 min. At this time approximately 6.0±1.4% (mean, SD) of radioactivity injected was present in brain.

[^{11}C]PE2I provided high-contrast images in which the highest uptake was observed in the striatum, with intermediate uptake in the midbrain, low uptake in the thalamus and hypothalamus and very low binding in the cerebellum and neocortex (Fig. 2a). The volume-rendered [^{11}C]PE2I images not only demonstrated the DAT-rich regions but also confirmed the lack of evident DAT binding in the neocortex (Fig. 2b).

The radioactivity ratio (mean±SD) of the putamen and midbrain to the cerebellum was 10.2±0.9 and 2.9±0.4, respectively, at the end of measurement (frame 57–63 min). The TACs for the thalamus and cerebral cortices had profiles similar to that for the cerebellum (Fig. 3). Due to the low radioactivity ratio in the thalamus and the cerebral cortex, these regions were excluded from further detailed analysis.

The rapid decrease in radioactivity in plasma during the first 5 min after i.v. injection was followed by a phase with a slower rate of decrease (Fig. 4). The fraction of unmetabolised [^{11}C]PE2I in plasma decreased rapidly and was 12.5±4.4% (mean±SD) at 40 min (Fig. 4, inset). The HPLC chromatogram revealed two labelled metabolites. The metabolites (I, II) were more polar than the parent compound (Fig. 5).

Kinetic compartment analyses

For all regions, the 2-CM and the 3-CM were fitted to experimental data using the metabolite-corrected arterial plasma curve as an input function (Fig. 4). Multi-exponential function was used to fit the metabolite fraction values.

The TACs for regional [^{11}C]PE2I binding could be described both with the 2-CM and with the 3-CM (Fig. 6). The results of individual single rate constants for the 2-CM and 3-CM are given in Tables 1 (for the putamen) and 2 (for the cerebellum). The ratio of K_1/k_2 obtained by the 3-CM

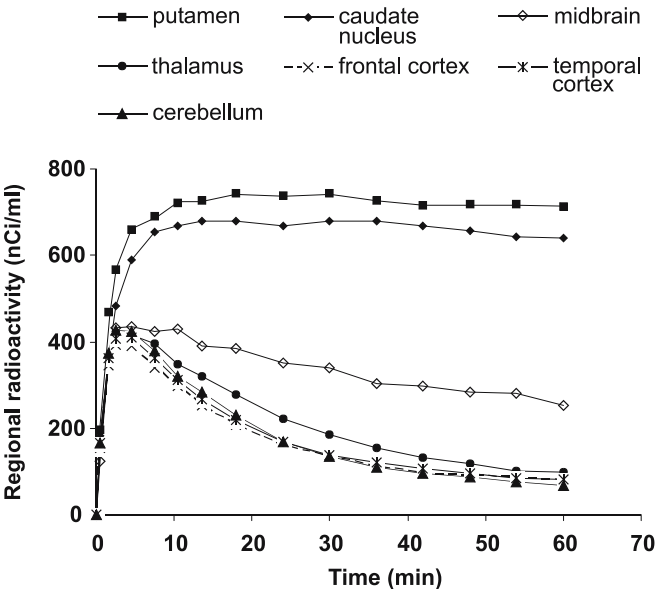

Fig. 3. TACs for regional brain radioactivity after i.v. injection of 280 MBq of [^{11}C]PE2I in one subject

ranged from 1.9 to 9.8 in the putamen, from 2.4 to 7.2 in the caudate and from 1.5 to 9.2 in the midbrain. K_1/k_2' obtained by the 2-CM for the cerebellum ranged from 2.4 to 4.9.

The comparison of fitted TACs between the models showed that the 3-CM was statistically preferred to describe kinetics of [^{11}C]PE2I in the putamen in three out of eight subjects, in the caudate nucleus in one subject, in the midbrain in four out of eight subjects, and in the cerebellum in seven out of eight subjects (examples presented in Tables 1 and 2). The rate constants derived from the 3-CM can be used to calculate the curves for the C_b and C_n, as

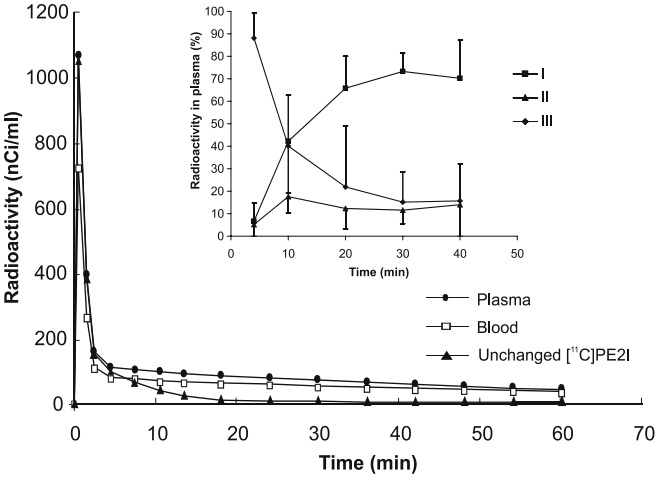

Fig. 4. TACs for radioactivity in whole blood and plasma as well as the calculated TAC for unchanged [^{11}C]PE2I obtained after i.v. injection of [^{11}C]PE2I in one subject. Data points represent sampling time. *Inset*: time course for the fraction (%) of radioactivity in plasma that represents unchanged [^{11}C]PE2I in eight human subjects (mean, SD)

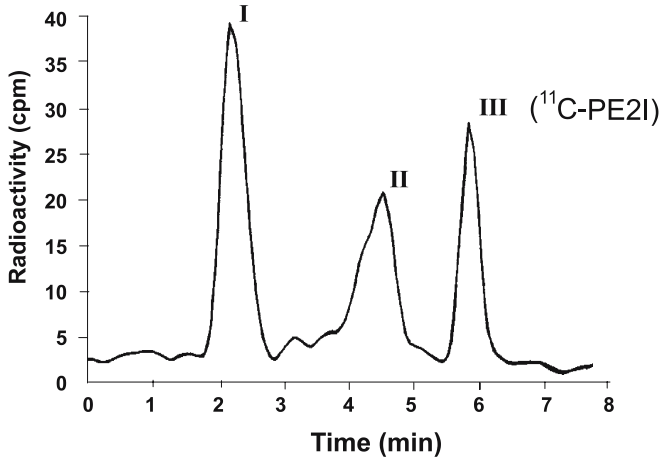

Fig. 5. Radiochromatogram from gradient HPLC analysis of human plasma at 10 min after i.v. injection of [^{11}C]PE2I (peak III). Peaks I and II represent labelled metabolites that are more polar than unchanged [^{11}C]PE2I

seen in Fig. 7. The time curve for the C_n in the putamen is initially lower than that for the cerebellum, but approaches the curve for the cerebellum with time [33].

The BPs obtained by kinetic analysis ranged from 7.4 to 20.1 in the putamen, from 11.3 to 17.6 in the caudate nucleus and from 1.0 to 5.4 in the midbrain (mean and SD values presented in Table 3).

There was no significant difference between DV obtained using the 2-CM ($DV_{2\text{-}CM}$) and DV obtained using the 3-CM (DV_{total}) (Table 4). $DV_{2\text{-}CM}$ and DV_{total} values correlated significantly for all regions ($p<0.0001$). The individual differences between $DV_{2\text{-}CM}$ and DV_{total} in the putamen ranged from −27% to 16% (mean±SD −0.4± 14.6%), in the caudate nucleus from −16% to 43% (9.1± 22.8%), in the midbrain from −1.7% to 0.2% (−0.5±0.6%) and in the cerebellum from −1.2% to −0.1% (−0.5±0.4%). An additional

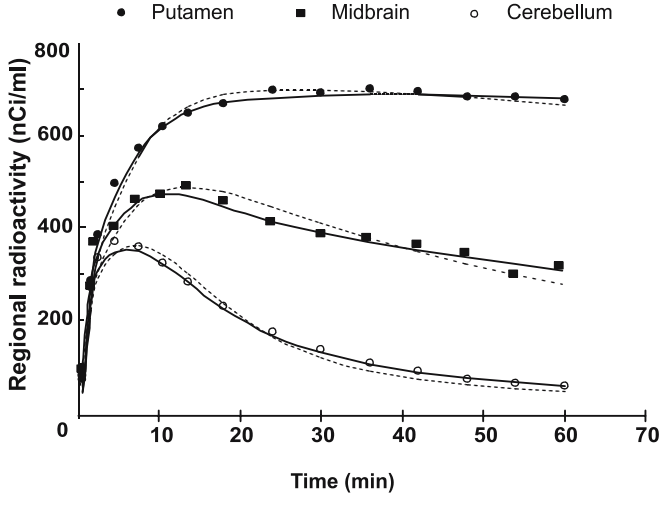

Fig. 6. Experimental values for regional radioactivity in the putamen, midbrain and cerebellum in one subject, with the corresponding fitted curves obtained by the 2-CM (---) and 3-CM (–)

observation was the high distribution volume for the cerebellum, DV_{total}, ranging from 2.7 to 5.2 (Table 4).

Linear graphical analyses

The linear graphical analysis [25] yielded a linear phase for all regions (Fig. 8). The slope of the fitted line was used to obtain DV_{Logan}, the regional distribution volumes. The BP values obtained by the linear graphical analysis [$BP_{Logan(kinetic)}$] ranged from 7.8 to 15.3 for the putamen, from 11.3 to 17.6 for the caudate nucleus and from 1.0 to 2.3 for the midbrain and were independent of the time interval used for the analysis (Table 3). The results of linear graphical analysis using cerebellum as an input function, $BP_{Logan(reference)}$, showed lower values for the striatum (Table 3) and were dependent on the time of the starting frame both in the caudate and in the putamen [e.g. for the putamen the BP values (mean±SD) were as follows: for the time interval 24–60 min, BP=6.0±0.72; 30–60 min, BP=6.62±0.71; 36–60 min, BP=6.9±0.98; 42–60 min, BP=7.14±1.1 and 46–60 min, BP=7.50±1.4]. The shortest time interval used approached but did not reach the BP values acquired using the arterial input function.

Simple reference tissue model

In the simplified reference tissue model (SRTM), binding potentials were computed using the cerebellum as a reference region for non-displaceable (free + non-specific) [^{11}C]PE2I binding in the brain. The BP values obtained by SRTM were lower than those obtained with the two kinetic methods (Table 3). The lowest coefficient of variance (COV) was consistently observed for the BPs obtained with the SRTM (BP_{SRTM}).

The BP was also obtained using the ratio between distribution volumes in the ROI and the reference region ($BP=DV_{ROI}/DV_{REF}-1$). The BPs for the caudate nucleus varied from 12.2 to 18.6 (14.7±2.3, COV 15%), for the putamen from 9.5 to 17.5 (14.3±2.7, COV 18%) and for the midbrain from 1.4 to 5.2 (3.6±1.8, COV 50%).

The specific radioactivity (SA) of [^{11}C]PE2I at the time of injection and the injected mass varied between the subjects and its approximate effect on BP values was investigated. Briefly, the average values for C_b and C_n obtained from 40 to 60 min after injection were divided by the specific radioactivity and the free and specifically bound radioligand concentrations (B and F) were obtained. There was a negative relationship between injected mass and B/F values (e.g. in the putamen: $r^2=0.61$; $r=-0.78$; $p=0.02$).

Comparison between the analyses

There were highly significant correlations between DV_{total} and DV_{Logan} for both the caudate nucleus and the putamen ($r=0.96$, $p=0.0001$). There were no statistically significant

Table 1. Comparison of the 2-CM and 3-CM for description of [^{11} C]PE2I binding in the putamen of eight healthy subjects

Subject, model		K_1 (ml/ml/min)	k_2 (min^{-1})	k_3 (min^{-1})	k_4 (min^{-1})	RSS	AIC	SC	F statistics (p value)
1	2-CM	0.27	0.005	–	–	10,501	143	144	<0.01
	3-CM	0.34	0.09	0.25	0.02	4,248	133	136	
2	2-CM	0.36	0.003	–	–	8,300	139	141	ns
	3-CM	0.43	0.07	0.45	–	9,217	145	148	
3	2-CM	0.30	0.002	–	–	4,815	114	115	ns
	3-CM	0.34	0.04	0.42	–	5,614	120	122	
4	2-CM	0.25	0.006	–	–	2,319	120	122	ns
	3-CM	0.32	0.11	0.53	–	3,681	131	134	
5	2-CM	0.29	0.005	–	–	2,606	122	123	<0.05
	3-CM	0.37	0.09	0.28	–	1,466	117	120	
6	2-CM	0.36	0.009	–	–	2,644	122	124	ns
	3-CM	0.48	0.17	0.52	–	3,028	128	131	
7	2-CM	0.23	0.008	–	–	958	107	108	ns
	3-CM	0.30	0.12	0.42	–	936	111	113	
8	2-CM	0.26	0.009	–	–	9,457	141	125	<0.001
	3-CM	0.35	0.10	0.20	–	2,453	143	128	
Mean (SD)									
–	2-CM	0.29 (0.05)	0.006 (0.003)	–	–	–	–	–	–
	3-CM	0.36 (0.05)	0.08 (0.04)	0.36 (0.13)	–	–	–	–	–

2-CM two-compartment model, *3-CM* three-compartment model, *RSS* residual square sum, *AIC* Akaike information criteria, *SC* Schwartz criteria, *ns* non-significant

correlations between the BPs quantified using the 3-CM and the SRTM, or between linear graphical analyses for any of the striatal regions. The relationship between BP values in the midbrain was significant for DV_{total}vs DV_{Logan} (r=0.72, p=0.05) and there was a trend towards a positive relationship for k_3/k_4 vs BP_{SRTM} (r=0.61, p=0.09) and $BP_{Logan\ (kinetic)}$vs $BP_{Logan(reference)}$ (r=0.64, p=0.09).

Table 2. Comparison of the 2-CM and 3-CM for description of [^{11} C]PE2I binding in the cerebellum of eight healthy subjects

Subject, model		K_1 (ml/ml/min)	k_2 (min^{-1})	k_5 (min^{-1})	k_6(min^{-1})	RSS	AIC	SC	F statistics (p value)
1	2-CM	0.21	0.07	–	–	14,190	147	149	<0.0001
	3-CM	0.26	0.13	0.05	0.07	3,889	132	135	
2	2-CM	0.31	0.06	–	–	11,145	144	145	<0.05
	3-CM	0.35	0.09	0.03	0.08	5,542	137	140	
3	2-CM	0.26	0.05	–	–	10,574	143	144	<0.005
	3-CM	0.29	0.08	0.02	0.03	3,836	132	135	
4	2-CM	0.18	0.08	–	–	4,650	131	132	<0.025
	3-CM	0.20	0.10	0.01	0.09	2,345	124	127	
5	2-CM	0.22	0.07	–	–	2,882	128	129	<0.00025
	3-CM	0.26	0.11	0.03	0.04	826	109	112	
6	2-CM	0.29	0.07	–	–	1,986	118	119	ns
	3-CM	0.31	0.09	0.01	0.08	1,651	119	122	
7	2-CM	0.22	0.08	–	–	1,530	114	115	<0.025
	3-CM	0.24	0.11	0.02	0.06	911	110	113	
8	2-CM	0.25	0.10	–	–	7,813	138	140	<0.0025
	3-CM	0.31	0.16	0.04	0.09	2,583	126	129	
Mean (SD)									
	2-CM	0.24 (0.04)	0.07 (0.01)						
	3-CM	0.28 (0.05)	0.10 (0.03)	0.02 (0.01)	0.06 (0.03)				

2-CM two-compartment model, *3-CM* three-compartment model, *RSS* residual square sum, *AIC* Akaike information criteria, *SC* Schwartz criteria, *ns* non-significant

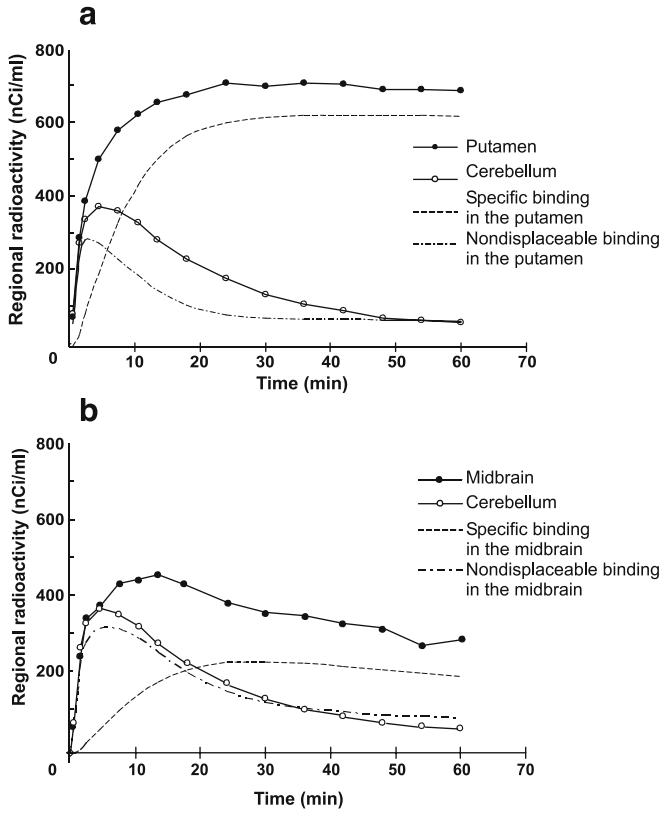

Fig. 7. The curves for the specific binding (C_b) and non-specific binding (C_{ns}) in the putamen (**a**) and midbrain (**b**) calculated using the rate constants obtained from the three-compartment model

Discussion

The present study demonstrated that the new PET radioligand [^{11}C]PE2I provides high-contrast images of DAT binding in the striatum and intermediate-contrast images in the midbrain, whereas low binding was seen in the thalamus and hypothalamus and very low binding in the cerebellum and neocortex. The demonstrated regional distribution of [^{11}C]PE2I binding to DAT in vivo is consistent with the binding pattern demonstrated by previous autoradiographic studies in the human brain in vitro using ^{125}I-labelled PE2I [9, 34]. In addition, the results correspond to the findings of in situ hybridisation studies, which have shown distinct DAT expression in terminals in the striatum, on dendrites and cell bodies of the substantia nigra and on ventral tegmentum neurons [35].

A number of radioligands have been developed during the past decade for PET imaging of DAT distribution in the human brain. A common drawback of these ligands has been a similar affinity to other monoamines, e.g. to the serotonin ([^{123}I]β-CIT) or noradrenaline transporters ([^{11}C] nomifensine) [36, 37]. [^{11}C]PE2I is a ligand for the DAT which has moderate affinity to DAT (K_d=4 n*M*) and about 30-fold lower affinity to serotonin (SERT) and noradrenaline transporters (NET) [38, 39]. The favourable selectivity of [^{11}C]PE2I is consistent with the high contrast of the images, which show no DAT binding in the neocortex. This quality is of particular value for the investigation of DAT binding in the midbrain, where SERT density is high.

Moreover, [^{11}C]PE2I has rather a favourable distribution to brain. After intravenous injection of the radioligand, 6±1.4% of radioactivity was present in the brain. This distribution is higher than that of other radioligands for DAT (e.g. a value of 2.5% is observed for [^{18}F]β-CIT-FP [40]) and also higher than that of the other reference ligands for central neuroreceptors, such as [^{11}C]WAY-100635, [^{11}C]SCH 23390 and [^{11}C]raclopride [20, 41, 42]. The favourable brain distribution implies that good imaging statistics can be obtained at relatively low radiation exposure. This is of value when using several radioligands in the same subject and of particular advantage in studies on children.

Cerebellum

Cerebellum was chosen as a reference region when using reference methods to quantify [^{11}C]PE2I binding. There is no evident visual distinction between the 2-CM and the 3-CM fit to experimental data. The statistical comparison, however, indicates that [^{11}C]PE2I binding in the cerebellum is better characterised by the 3-CM. This observation

Table 3. BP values for [^{11} C]PE2I calculated by kinetic and reference tissue approaches

Brain region	Kinetic approaches				Reference tissue approaches			
	Kinetic 3-CM analysis (k_3/k_4)		Linear graphical analysis [$BP_{Logan(kinetic)}$]		Linear graphical analysis [$BP_{Logan(reference)}$]		SRTM	
	Mean (SD)	COV (%)	Mean (SD)	COV (%)	Mean (SD)	COV (%)	Mean (SD)	COV (%)
Putamen	11.0 (4.4)	39	12.7 (2.7)	21	7.9 (1.4)	18	8.5 (0.8)	19
Caudate nucleus	14.6 (4.9)	33	12.1 (3.3)	27	6.7 (1.2)	18	7.5 (1.41)	9
Midbrain	2.5 (1.7)	69	1.7 (0.5)	26	1.1 (0.4)	36	1.5 (0.3)	19
Cerebellar cortex	0.5[a] (0.2)	40	–	–	–	–	–	–

COV coefficient of variance, *SRTM* simplified reference tissues model, *3-CM* three-compartment model
[a] k_5/k_6

Table 4. The DV obtained by the 2-CM, the 3-CM and the linear graphical analysis method

Brain region	DV $_{2\text{-CM}}$	DV $_{total}$	DV $_{Logan}$
Caudate	96.2 (100.4)	69.19 (49.31)	49.97 (23.43)
COV (%)	104	71	47
Putamen	65.3 (47.1)	62.12 (35.15)	51.63 (19.12)
COV (%)	72	56	37
Midbrain	8.2 (3.0)	12.1 (5.49)	8.91 (2.79)
COV (%)	37	45	31
Cerebellar cortex	3.4 (1.0)	3.89 (1.02)	3.74 (1.02)
COV (%)	29	27	27

Values presented as mean (SD)
COV coefficient of variance, *2-CM* two-compartment model; $DV_{2\text{-CM}}=K_1/k_2$ is the distribution volume for the 2-CM; $DV_{total}=K_1/k_2(1+k_3/k_4)$ is the distribution volume for the 3-CM; DV_{Logan} is the distribution volume obtained using the arterial input curve and linear graphical analysis

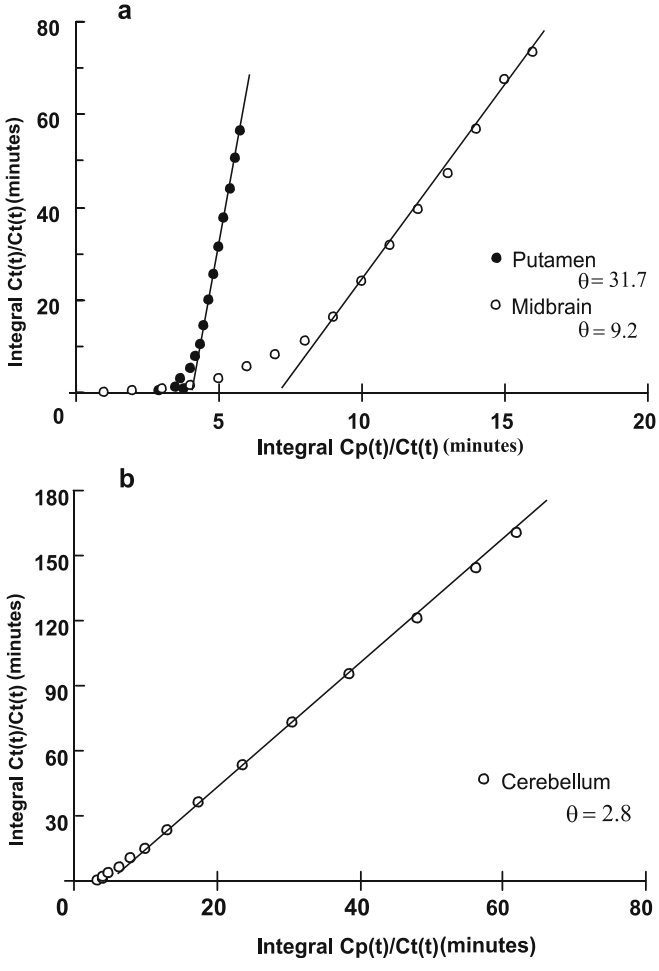

Fig. 8. Linear graphical analyses of [^{11}C]PE2I binding in the putamen, midbrain (**a**) and cerebellum (**b**) of one subject

suggests the presence of an additional compartment in the cerebellum, representing either specific (C_b) or non-specific (C_{ns}) binding. Studies on human brain tissue in vitro have shown that the cerebellum is a region with no evident DAT binding [9, 43], and expression of mRNA for DAT has been reported only in the vermis, and not in the cerebellar hemispheres [44]. Our previous PET study in monkeys showed that [^{11}C]PE2I binding in the cerebellum could not be inhibited by displacement or pretreatment with cocaine [10]. Thus, it is not likely that the identified third compartment in the cerebellum represents specific [^{11}C]PE2I binding to DAT.

Alternatively, the third compartment may represent non-specific binding, i.e. a radioactive metabolite might pass the blood-brain barrier. The two major labelled metabolites of [^{11}C]PE2I are more polar, however, and thus less likely to pass the blood-brain barrier. Furthermore, experimental animal studies and studies in vitro have shown that the main routes of metabolism of PE2I are aromatic hydroxylation at the phenyl ring and N-desalkylation, suggesting that in PET studies in humans the main metabolites of [^{11}C]PE2I retain their labelling [45]. The observation of a possible additional compartment in the cerebellum calls for identification of labelled metabolites and separate PET studies to examine the distribution of labelled metabolites to brain.

Striatum

The kinetic compartment analysis showed high inter-individual variability of the rate constants, as seen from the high COV values (Table 3). The poor reliability in the estimation of single rate constants may be one reason for the threefold range in the subsequently calculated individual k_3/k_4 values. Quantifications may have been influenced by the reliability of the estimates of [^{11}C]PE2I and its metabolites in plasma, the curves being based on a few observations only. In addition, the rate of metabolism of [^{11}C]PE2I was characterised by large inter-individual variability (Fig. 4, inset). These factors may have influenced the statistical estimations of the preferred compartment model. However, the range in k_3/k_4 may also include a biological inter-individual variability in DAT density. This view is indirectly supported by an earlier detailed study of another biomarker of the dopamine system. A threefold range was reported for the dopamine D_2 receptor density in a group of 20 healthy adults [46]. The threefold range in BP for [^{11}C]PE2I observed in the present study may thus represent true biological variability.

The BP values in the striatum obtained using the arterial input function were about 30% higher than the values obtained using reference tissue approaches. The limited reliability and validity of the metabolite correction and thus a possibly overcorrected arterial plasma input curve may be one reason for the higher BP values obtained using the arterial input function. Another possible explanation is that some assumptions of the reference methods may have been violated [26]. The regional differences for K_1/k_2 values also challenge a main assumption of the SRTM [26]. In addition, only in three out of eight subjects did the TACs reach equilibrium, suggesting that the data acquisition time

of 60 min may not be sufficient for accurate quantification of BPs. These conditions may be a reason for the different BP values obtained using reference tissue approaches.

Of special interest is the discrepancy between BP values obtained using linear graphical analyses with different input functions. In addition to the previously mentioned limited precision of measurements, different results in linear graphical analyses may be viewed in relation to the acquisition time needed for reliable estimates. BP values obtained using the arterial input function yielded the same results from 24 min onwards, while results using the reference region showed time dependency throughout all the measurement. This finding is consistent with a previous SPECT study [47] using [^{123}I]PE2I, suggesting that measurements in the striatum require a prolonged data acquisition time of up to 90 min.

A lack of correlation between the BPs quantified by different approaches for other ligands has been observed by several authors [24, 48]. The suggested reason for this has been a relatively poor separation between the 2-CM and 3-CM in striatal regions with high receptor density. Moderate affinity of [^{11}C]PE2I and high variability of specific radioactivity injected may also have contributed to the higher differences in BP values [49]. Another suggestion is that increasing additive statistical noise of the PET system leads to underestimation of the distribution volume ratio (DVR) in receptor-dense regions [50].

In clinical PET studies there is a need to avoid invasive procedures such as arterial blood sampling. Indirect methods using the cerebellum as a reference region may thus be more applicable than direct ones. Among the indirect quantitative approaches, the simplified reference tissue method yielded the lowest coefficient of variance and may thus be used for clinical purposes, provided that the data are acquired for a longer period (90 min).

Midbrain

The midbrain is a brain region of particular interest, representing the origin of dopaminergic innervation and being implicated in the regulation of normal behaviours as well as in the pathophysiology of neurological disorders (e.g. Parkinson's disease [44]). The particular potential of [^{11}C]PE2I to identify selective DAT binding in the substantia nigra/ventral tegmentum has previously been mentioned in PET and SPECT studies [10, 37, 51, 52], but no attempts have been made to quantify the radioligand binding. In the present study there was a twofold signal-to-background ratio for [^{11}C]PE2I binding in the midbrain. The 3-CM was statistically preferred for description of TACs in the midbrain in four out of eight subjects. It is worth noting, however, that inter-individual variability of BP values was high (COV 69%) as compared with BPs obtained in other regions (Table 3). This could be explained partly by the higher noise effects on error size in a small region such as the midbrain. However, despite less favourable reliability, the present analysis of [^{11}C]PE2I binding in the midbrain supports the idea that DAT expression in the midbrain is an area that can be addressed in future applied studies on the pathophysiology of neuropsychiatric disorders.

Conclusion

The present study in eight adult subjects corroborates a previous case report on the favourable signal-to-background ratio for [^{11}C]PE2I binding to DAT in the human striatum and midbrain. [^{11}C]PE2I binding can be interpreted using a kinetic analysis with a metabolite-corrected arterial plasma input function. However, it cannot be excluded that radiolabelled metabolites may represent a small component of total [^{11}C]PE2I binding in the brain. The simplified reference tissue model or other reference methods using cerebellum time-activity curves with prolonged data acquisition time and high specific radioactivity at injection time may be used for estimation of [^{11}C]PE2I binding in clinical studies. A particular advantage of [^{11}C]PE2I is the possibility of quantifying binding to DAT in the midbrain, a region containing dopaminergic cell bodies and of central interest in the pathogenesis of several neuropsychiatric disorders.

Acknowledgements. This work was supported by grants from the Swedish Research Council (09114/15A). Aurelija Jucaite was sponsored by The Frimurare Barnhuset, Sunnerdahl Handikapp, Sällskapet Barnavård, Professor Bror Gardelius Memorial Foundation. The authors would like to thank the members of the Stockholm PET group, and in particular Kjerstin Lind and Arsalan Amir, for their participation in data acquisition and for their technical assistance.

References

1. Gulley JM, Zahniser NR. Rapid regulation of dopamine transporter function by substrates, blockers and presynaptic receptor ligands. Eur J Pharmacol 2003;31(479):139–152
2. Antonini A, Moresco RM, Gobbo C, De Notaris R, Panzacchi A, Barone P, et al. The status of dopamine nerve terminals in Parkinson's disease and essential tremor: a PET study with the tracer [11-C]FE-CIT. Neurol Sci 2000;22:47–48
3. Ginovart N, Lundin A, Farde L, Halldin C, Backman L, Swahn CG, et al. PET study of the pre- and post-synaptic dopaminergic markers for the neurodegenerative process in Huntington's disease. Brain 1997;120:503–514
4. Laakso A, Bergman J, Haaparanta M, Vilkman H, Solin O, Syvalahti E, et al. Decreased striatal dopamine transporter binding in vivo in chronic schizophrenia. Schizophr Res 2001;52:115–120
5. Dresel S, Krause J, Krause K-H, LaFougere C, Brinkbäumer K, Kung HF, et al. Attention deficit hyperactivity disorder: binding of [^{99m}Tc]TRODAT-1 to the dopamine transporter before and after methylphenidate treatment. Eur J Nucl Med 2000;27:1518–1524
6. Jucaite A, Fernell E, Halldin C, Forssberg H, Farde L. Reduced midbrain dopamine transporter binding in male adolescents with ADHD; association between striatal dopamine markers and motor hyperactivity. Biol Psychiatry 2005;57(3):229–238

7. Volkow ND, Wang GJ, Fowler JS, Logan J, Francheschi D, Maynard L, et al. Relationship between blockade of dopamine transporters by oral methylphenidate and increase in the extracellular dopamine: therapeutic implications. Synapse 2002;43: 181–187
8. Emond P, Garreau L, Chalon S, Boazi M, Caillet M, Bricard J, et al. Synthesis and ligand binding of nortropane derivatives: N-substituted-2-carbomethoxy-3-(4'-iodophenyl)nortropane and N-(3-iodoprop-2E-enyl)-2-carbomethoxy-3-(3',4'-disubstituted phenyl)nortropane. New affinity and selectivity compounds for the dopamine transporter. J Med Chem 1997; 40:1366-1372
9. Hall H, Halldin C, Guilloteau D, Chalon S, Emond P, Besnard J, et al. Visualization of the dopamine transporter in the human brain postmortem with the new selective ligand [^{125}I]PE2I. Neuroimage 1999;9:108–116
10. Halldin C, Erixon-Lindroth N, Pauli S, Chou YH, Okubo Y, Karlsson P, et al. [^{11}C]PE2I—a highly selective radioligand for PET-examination of the dopamine transporter in monkey and human brain. Eur J Nucl Med Mol Imaging 2003;30:1220–1230
11. Frost JJ, Douglass KH, Mayberg HS, Dannals RF, Links JM, Wilson AA, et al. Multicompartmental analysis of [^{11}C]-carfentanil binding to opiate receptors in humans measured by positron emission tomography. J Cereb Blood Flow Metab 1989;9:398–409
12. Wong D, Gjedde A, Wagner H Jr. Quantification of neuroreceptors in the living human brain. I. Irreversible binding of ligands. J Cereb Blood Flow Metab 1986;6:137–146
13. Mintun M, Raichle M, Kilbourn M, Wooten G, Welch M. A quantitative model for the in vivo assessment of drug binding sites with positron emission tomography. Ann Neurol 1984;15: 217–227
14. Huang S, Barrio J, Phelps M. Neuroreceptor assay with positron emission tomography. Equilibrium versus dynamic approaches. J Cereb Blood Flow Metab 1986;6:515–521
15. Caceci MS, Cacheris WP. Fitting curves to data, the Simplex algorithm in the answer. BYTE 1984;9:340–362
16. Perlmutter JS, Larson KB, Raichle ME, Markham J, Mintun MA, Kilbourn MR, et al. Strategies for in vivo measurement of receptor binding using positron emission tomography. J Cereb Blood Flow Metab 1986;6:154–169
17. Farde L, Eriksson L, Blomquist G, Halldin C. Kinetic analysis of central [^{11}C]raclopride binding to D_2-dopamine receptors studied by PET—a comparison to the equilibrium analysis. J Cereb Blood Flow Metab 1989;9:696–708
18. Koeppe RA, Holthoff VA, Frey KA, Kilbourn MR, Kuhl DE. Compartmental analysis of [^{11}C]flumazenil kinetics for the estimation of ligand transport rate and receptor distribution using positron emission tomography. J Cereb Blood Flow Metab 1991;11:735–744
19. Delforge J, Pappata S, Millet P, Samson Y, Bendriem B, Jobert A, Crouzel C, Syrota A. Quantification of benzodiazepine receptors in human brain using PET, [^{11}C]flumazenil, and a single-experiment protocol. J Cereb Blood Flow Metab 1995; 15:284–300
20. Farde L, Ito H, Swahn CG, Pike VW, Halldin C. Quantitative analyses of carbonyl-carbon-11-WAY-100635 binding to central 5-hydroxytryptamine-1A receptors in man. J Nucl Med 1998;39:1965–1971
21. Lammerstma AA, Bench CJ, Hume SP, Osman S, Gunn K, Brooks DJ, et al. Comparison of methods for analysis of clinical [^{11}C]raclopride studies. J Cereb Blood Flow Metab 1996;16:42–52
22. Akaike H. A new look at the statistical model identification. IEEE Trans Automat Contr 1974;19:716–723
23. Schwartz G. Estimating the dimension of a model. Ann Stat 1978;6:461–564
24. Hawkins R, Phelps M, Huand S-C. Effects of temporal sampling, glucose metabolic rates, and disruptions of the blood-brain barrier on the FDG model with and without a vascular compartment. Studies in human brain tumours with PET. J Cereb Blood Flow Metab 1986;6:170–183
25. Logan J, Fowler JS, Volkow ND, Wolf AP, Dewey SL, Schyler DJ, et al. Graphical analysis of reversible radioligand binding from time-activity measurements applied to [*N*-^{11}C-methyl]-(-)-cocaine PET studies in human subjects. J Cereb Blood Flow Metab 1990;10:740–747
26. Lammertsma AA, Hume SP. Simplified reference tissue model for PET receptor studies. Neuroimage 1996;4:153–155
27. Bergström M, Boëthius J, Eriksson L, Greitz T, Ribbe T, Widen L. Head fixation device for reproducible position alignment in transmission CT and positron emission tomography. J Comput Assist Tomogr 1981;5:136–141
28. Wienhard K, Dahlbom M, Eriksson L, Michel C, Bruckbauer T, Pietrzyk U, et al. The ECAT EXACT HR: performance of a new high resolution positron scanner. J Comput Assist Tomogr 1994;18:108–110
29. Eriksson L, Holte S, Bohm C, Kesselberg M, Hovander B. Automated blood sampling systems for positron emission tomography. IEEE Trans Nucl Sci 1988;35:703–707
30. Drebin RA, Carpenter L, Hanrahan P. Volume rendering. Comput Graph 1988;22:65–74
31. Toga AW. Three dimentional neuro imaging. New York: Raven Press; 1990
32. Pauli S, Sedvall G. Three-dimensional visualization of the benzodiazepine receptor population within a living human brain using PET and MRI. Eur Arch Psychiatry Clin Neurosci 1997;247:61–70
33. Olsson H, Halldin C, Farde L. Differentiation of extrastriatal dopamine D2 receptor density and affinity in the human brain using PET. NeuroImage 2004;22:794–803
34. Tupala E, Kuikka JT, Hall H, Bergstrom K, Sarkioja T, Rasanen P, et al. Measurement of the striatal dopamine transporter density and heterogeneity in type 1 alcoholics using human whole hemisphere autoradiography. Neuroimage 2001;14:87–94
35. Ciliax BJ, Drash GW, Staley JK, Haber S, Mobley CJ, Miller GW, et al. Immunocytochemical localization of the dopamine transporter in human brain. J Comp Neurol 1999;21(409): 38–56
36. Halldin C, Gulyas B, Langer O, Farde L. Brain radioligands—state of art and new trends. Q J Nucl Med 2001;45:139–152
37. Laruelle M, Slifstein M, Huang Y. Positron emission tomography: imaging and quantification of neurotransporter availability. Methods 2002;27:287–299
38. Chalon S, Emond P, Garreau L, Frangin Y, Mauclaire L, Guilloteau D, et al. Characterisation of the cocaine derivative PE2I, a high specific marker for imaging the dopamine transporter by SPECT. Eur J Nucl Med 1997;24:880
39. Gu XH, Zong R, Kula NS, Baldessarini RJ, Neumeyer JL. Synthesis and biological evaluation of a series of novel N- or O-fluoroalkyl derivatives of tropane: potential positron emission tomography (PET) imaging agents for the dopamine transporter. Bioorg Med Chem Lett 2001;11:3049–3053
40. Lundkvist C, Halldin C, Ginovart N, Swahn CG, Farde L. [^{18}F] beta-CIT-FP is superior to [^{11}C] beta-CIT-FP for quantitation of the dopamine transporter. Nucl Med Biol 1997;24:621–627
41. Karlsson P, Sedvall G, Halldin C, Swahn CG, Farde L. Evaluation of SCH 39166 as PET ligand for central D1 dopamine receptor binding and occupancy in man. Psychopharmacology (Berl) 1995;121:300–308
42. Farde L, Hall H, Ehrin E, Sedvall G. Quantitative analysis of D2 dopamine receptor binding in the living human brain by PET. Science 1986;231(4735):258–261

43. Madras BK, Gracz LM, Fahey MA, Elmaleh D, Meltzer PC, Liang AY, et al. Altropane, a SPECT or PET imaging probe for dopamine neurons: III. Human dopamine transporter in post-mortem normal and Parkinson's diseased brain. Synapse 1998;29:116–127
44. Hurley MJ, Mash DC, Jenner P. Markers for dopaminergic neurotransmission in the cerebellum in normal individuals and patients with Parkinson's disease examined by RT-PCR. Eur J Neurosci 2003;18:2668–2672
45. Schollborn-Peyronneau M, Pruvost A, Kuhnast B, Coulon C, Ottaviani M, Emond P, et al. Metabolism of PE2I and ^{11}C-PE2I, a high selective ligand for PET examination of the dopamine transporter. J Nucl Med 2005;346:347
46. Farde L, Hall H, Pauli S, Halldin C. Variability in D2-dopamine receptor density and affinity: a PET study with [^{11}C]raclopride in man. Synapse 1995;10:200–208
47. Pinborg LH, Videbaek C, Svarer C, Yndgaard S, Paulson OB, Knudsen GM. Quantification of [^{123}I]PE2I binding to dopamine transporters with SPET. Eur J Nucl Med Mol Imaging 2002;29:623–631
48. Olsson H, Halldin C, Swahn CG, Farde L. Quantification of [^{11}C] FLB 457 binding to extrastriatal dopamine receptors in the human brain. J Cereb Blood Flow Metab 1999;19(10):1164–1173
49. Olsson H, Halldin C, Farde L. Differentiation of extrastriatal dopamine D2 receptor density and affinity in the human brain using PET. Neuroimage 2004;22(2):794–803
50. Slifstein M, Laruelle M. Effects of statistical noise on graphic analysis of PET neuroreceptor studies. J Nucl Med 2000; 41:2083–2088
51. Moore RY. Organization of midbrain dopamine systems and the pathophysiology of Parkinson's disease. Parkinsonism Relat Disord Suppl 2003;2:S65–S71
52. Poyot T, Conde F, Gregoire MC, Frouin V, Coulon C, Fuseau C, et al. Anatomic and biochemical correlates of the dopamine transporter ligand ^{11}C-PE2I in normal and parkinsonian primates: comparison with 6-[^{18}F]fluoro-L-dopa. J Cereb Blood Flow Metab 2001;21:782–792